ANS RPSD 2018 - 20th Topical Meeting of the Radiation Protection & Shielding Division of ANS Santa Fe, NM, August 26 – 31, 2018, on CD-ROM, American Nuclear Society, LaGrange Park, IL (2018)



ADJOINT-ENABLED MULTIDIMENSIONAL OPTIMIZATION OF SATELLITE ELECTRON/PROTON SHIELDS

Shawn Pautz¹, Don Bruss¹, Brian Adams¹, Brian Franke¹, and Ethan Blansett¹

¹Sandia National Laboratories, Albuquerque, NM, 87185, 505-284-4291, sdpautz@sandia.gov

The design of satellites usually includes the objective of minimizing mass due to high launch costs, which is complicated by the need to protect sensitive electronics from the space radiation environment. There is growing interest in automated design optimization techniques to help achieve that objective. Traditional optimization approaches that rely exclusively on response functions (e.g. dose calculations) can be quite expensive when applied to transport problems. Previously we showed how adjointbased transport sensitivities used in conjunction with gradient-based optimization algorithms can be quite effective in designing mass-efficient electron/proton shields in one-dimensional slab geometries. In this paper we extend that work to two-dimensional Cartesian This consists primarily of deriving the geometries. sensitivities to geometric changes, given a particular prescription for parametrizing the shield geometry. We incorporate these sensitivities into our optimization process and demonstrate their effectiveness in such design calculations.

I. INTRODUCTION

Satellites in orbit around Earth encounter harsh radiation environments due to trapped electrons and/or protons. Electronics and other components often require shielding; the amount needed depends on the orbit and the mission lifetime. The mass of shielding adds to launch costs and/or subtracts from satellite capabilities, so there is motivation to optimize the shielding to minimize the mass. If multiple shielding materials are under consideration, the optimal design is not obvious due to competing physical processes.¹

In recent years there has been a growing body of work in the radiation transport community on the use of adjoint problems to inexpensively obtain sensitivities of output quantities of interest to various input parameters. In one strain of research these sensitivities have been derived by means of a Lagrangian approach.^{2,3} These sensitivities can be used directly, or through an intermediate response surface, to answer various analysis questions. In the works cited above and related work the emphasis has been on material sensitivities which have been used primarily to inform uncertainty quantification (UQ) studies.

Other recent work has also used adjoint problems to obtain sensitivities by means of a variational approach. In addition to material sensitivities this work has also

examined geometric changes. In Ref. 4 the sensitivities of k-eigenvalues to the radius of a sphere, the thickness of a shell, and the height or radius of a cylinder were derived. In Ref. 5 perturbation formulas for reaction rates and boundary fluxes with respect to the thickness of a slab or the radius of a sphere were derived, where "perturbations" may be large changes in the geometry (in essence the perturbation equations are extrapolations of the sensitivity equations defined for differential changes). Such equations are exact when the perturbations are "small", but are inexact for larger changes. In Refs. 6 and 7 perturbation equations for leakage fluxes due to nonspherical changes in spherical geometries were derived. In some cases, the equations are exact for small perturbations, but for other changes the equations are always approximations. In Refs. 8 and 9 the sensitivities of certain leakage fluxes with respect to the radii of spheres or the heights or radii of cylinders were used to perform least-squares optimization analyses to solve for up to three unknown geometric variables in an inverse problem.

Recently we have applied adjoint-based sensitivities to the question of design optimization for satellite shields. ¹⁰ We derived sensitivities to key design parameters for shielding in one-dimensional slab geometries by means of a Lagrangian analysis. We incorporated these sensitivities into a gradient-based optimization algorithm and demonstrated the effectiveness of this approach for the design of combined electron/proton satellite shields.

In the present work we extend the above approach to two-dimensional Cartesian geometries. Our previous work had derived sensitivities with respect to material changes that are valid for any geometries, so the current work focuses on geometry changes. This consists first in defining a parametrization of shield geometries that encompasses the desired design space and that is amenable to analysis. We then derive transport sensitivities with respect to changes in those geometric parameters. Finally, we incorporate those sensitivities into our design process and apply them to some problems of interest.

II. THEORY

In this section we present the theory of transport sensitivities and how they are used in design optimization calculations. First, we review the general theory of adjointbased transport sensitivities. Next, we describe our previous work in one-dimensional transport sensitivities as applied to satellite applications. Finally, we derive sensitivities for multi-dimensional geometries.

II.A. Previous Work

II.A.1. General Theory of Transport Sensitivities

We begin by briefly reviewing previous work that derived a general expression for sensitivities.³ The general problem to be considered is

$$\Omega \cdot \nabla \psi + \sigma_t(r, E)\psi = \int_{E'} dE' \int_{4\pi} d\Omega' \sigma_s(r, \Omega' \to \Omega, E' \to E)\psi(r, \Omega', E') + q$$
(1a)

$$\psi = \psi_b(r, \Omega, E), \{r \in \partial D | \Omega \cdot \vec{n} < 0\}$$
 (1b)

$$R = \int_{D} dr \int_{E} dE \int_{4\pi} d\Omega \psi(r, \Omega, E) q^{\dagger}(r, E)$$
 (1c)

Equation (1a) is the familiar Boltzmann transport equation with boundary conditions given by Eq. (1b) and response given by Eq. (1c). In the case of satellite shielding one important response is dose to a component with $q^{\dagger} = \sigma_d(r, E)/V$.

For simplicity of notation we may express Eq. (1a) as

$$L\psi + C\psi = S\psi + q \tag{2}$$

We also define a general inner product

$$\int_{D} dr \int_{E} dE \int_{4\pi} d\Omega ab \equiv \langle a, b \rangle$$
 (3)

We introduce a Lagrangian and its derivative with respect to a general input parameter p:

$$\mathcal{L} = \langle \psi, q^{\dagger} \rangle - \langle \psi^{\dagger}, L\psi + C\psi - S\psi - q \rangle$$
 (4a)

$$\frac{d\mathcal{L}}{dp} = \frac{\partial \mathcal{L}}{\partial p} + \frac{\partial \mathcal{L}}{\partial \psi} \frac{\partial \psi}{\partial p} \tag{4b}$$

After combining Eqs. (2)-(4) and performing various manipulations it can be shown that

$$\frac{d\mathcal{L}}{dp} = \left[\left\langle \psi, \frac{\partial q^{\dagger}}{\partial p} \right\rangle + \left\langle \psi^{\dagger}, \frac{\partial q}{\partial p} \right\rangle - \left\langle \psi^{\dagger}, \left(\frac{\partial}{\partial p} (L + C - S) \right) \psi \right\rangle + \left\langle \frac{\partial \psi}{\partial p}, q^{\dagger} - \left(L^{\dagger} + C^{\dagger} - S^{\dagger} \right) \psi^{\dagger} \right\rangle + \left\langle \frac{\partial \psi^{\dagger}}{\partial p}, q - (L + C - S) \psi \right\rangle \right] + \left[\left\langle I, q^{\dagger} - \left(L^{\dagger} + C^{\dagger} - S^{\dagger} \right) \psi^{\dagger} \right\rangle + \left\langle \frac{\partial \psi^{\dagger}}{\partial \psi}, q - (L + C - S) \psi \right\rangle \right] \frac{\partial \psi}{\partial p} \tag{5}$$

If we impose the condition that ψ and ψ^{\dagger} satisfy the following forward and adjoint problems:

$$(L+C-S)\psi = q \tag{6a}$$

$$(L^{\dagger} + C^{\dagger} - S^{\dagger})\psi^{\dagger} = q^{\dagger} \tag{6b}$$

then Eq. (5) reduces to

$$\frac{d\mathcal{L}}{dp} = \left[\left\langle \psi, \frac{\partial q^{\dagger}}{\partial p} \right\rangle + \left\langle \psi^{\dagger}, \frac{\partial q}{\partial p} \right\rangle - \left\langle \psi^{\dagger}, \left(\frac{\partial}{\partial p} \left(L + C - S \right) \right) \psi \right\rangle \right] = \frac{dR}{dp}$$
(7)

Eq. (7) indicates that the sensitivity of a response R to a parameter p is given by inner products involving a forward solution ψ , an adjoint solution ψ^{\dagger} , and derivatives of transport operators and sources; no other output quantities or derivatives are needed. The same ψ and ψ^{\dagger} are needed for any arbitrary p; only the inner product varies for different parameters. Thus, two transport solves in conjunction with numerous relatively inexpensive inner products may be used to obtain any number of sensitivities. This reduction in the number of transport calculations (relative to finite difference techniques) is the key to potential improved algorithmic performance.

II.A.2. Application to Satellite Shield Design in One-Dimensional Slab Geometry

In previously reported work we derived transport sensitivities for relevant design parameters in one-dimensional satellite shielding applications.¹⁰ We present here the essential results of that analysis.

One important design parameter is material selection. We assumed in our previous work that a satellite shielding region consists of a homogeneous mixture of one or more base materials (e.g. elements). We do not necessarily envision that one would be able to use such a mixture in a real application, but this approach simplifies the analysis. With the above assumption we derived the following expression for the sensitivity of a transport response (e.g. dose to an electronic component) to the volume fraction $p_{m,i}$ of material m in region i:

$$\begin{split} \frac{dR}{dp_{m,i}} &= -\langle \psi_{g}^{\dagger}, \left(\frac{\partial C}{\partial p_{m,i}}\right) \psi_{g'} \rangle + \langle \psi_{g}^{\dagger}, \left(\frac{\partial S}{\partial p_{m,i}}\right) \psi_{g'} \rangle \\ &= \langle \psi_{g}^{\dagger}, \sum_{g'} M \Sigma_{g'g,m} D \, \psi_{g'} \rangle_{D_{i}} \\ &+ \sigma_{\delta,gg,m} \langle \psi_{g}^{\dagger}, (I-MD) \psi_{g} \rangle_{D_{i}} \\ &- \sigma_{t,g,m} \langle \psi_{g}^{\dagger}, \psi_{g} \rangle_{D_{i}} \end{split} \tag{8}$$

We note that the above equation is valid for general geometries.

Another important design parameter is the physical geometry. The sensitivity of a transport response to the location x_i of an interface between two constant-density

material regions 1 and 2 (one of which could be a void region) is given by:

$$\begin{split} \frac{dR}{dx_i} &= -\langle \psi_g^\dagger, \left(\frac{\partial C}{\partial x_i}\right) \psi_{g'} \rangle + \langle \psi_{g'}^\dagger, \left(\frac{\partial S}{\partial x_i}\right) \psi_{g'} \rangle + \langle \psi_{g'}, \frac{\partial q^\dagger}{\partial x_i} \rangle \\ &= \sum_g \sum_m p_{m,2} \left(\sigma_{t,g,m,2} - \sigma_{\delta,gg,m,2}\right) \int\limits_{4\pi} d\Omega \psi_g^\dagger(x_i, \Omega) \psi_g(x_i, \Omega) \\ &- \sum_g \sum_m p_{m,1} \left(\sigma_{t,g,m,1} - \sigma_{\delta,gg,m,1}\right) \int\limits_{4\pi} d\Omega \psi_g^\dagger(x_i, \Omega) \psi_g(x_i, \Omega) \\ &+ \sum_g \int\limits_{4\pi} d\Omega \psi_g^\dagger(x_i, \Omega) \sum_{g'} \sum_m p_{m,1} M\left(\Sigma_{g'g,m,1} - \delta_{g'g} \sigma_{\delta,g'g,m,1} I\right) D \psi_{g'}(x_i, \Omega) \\ &- \sum_g \int\limits_{4\pi} d\Omega \psi_g^\dagger(x_i, \Omega) \sum_{g'} \sum_m p_{m,2} M\left(\Sigma_{g'g,m,2} - \delta_{g'g} \sigma_{\delta,g'g,m,2} I\right) D \psi_{g'}(x_i, \Omega) \\ &+ \frac{1}{\rho_1 V_1} \sum_g \sigma_{d,g,1} \int\limits_{4\pi} d\Omega \psi_g(x_i, \Omega) - \frac{1}{\rho_1 V_1^2} \sum_g \sigma_{d,g,1} \int\limits_{4\pi} d\Omega \int\limits_{D1} dr \psi_g(r, \Omega) \\ &- \frac{1}{\rho_2 V_2} \sum_g \sigma_{d,g,2} \int\limits_{4\pi} d\Omega \psi_g(x_i, \Omega) + \frac{1}{\rho_2 V_2^2} \sum_g \sigma_{d,g,2} \int\limits_{4\pi} d\Omega \int\limits_{D2} dr \psi_g(r, \Omega) \end{aligned} \tag{9}$$

The above expression is valid only for one-dimensional slab geometries.

II.B. Extension to Multidimensional Analysis

In this subsection we extend our previous work to twodimensional Cartesian geometries. As noted earlier the expression we derived for the sensitivities to materials is valid for all geometries. Therefore, we will focus on the sensitivities to geometrical factors.

There are numerous ways that one could parametrize geometries, which will affect the expression for geometric sensitivities. For our purposes we will focus on the situation that we depict in Figure 1. Here we show two material regions (with arbitrary outer boundaries depicted by the thin solid curves), with the interface between them shown as a thick dashed curve. That interface is defined by several "control" points (we have arbitrarily chosen six points for this example), with a line segment connecting adjacent points defining the interface. We have chosen a "central" point p_c , with rays r_1 through r_m emanating from that point and passing through the points that define the interface. We may modify the geometry by allowing each point defining the interface to move along its ray towards or away from p_c, subject to the constraints that it must stay within the two material regions. The material regions may or may not completely surround p_c; in this example they do

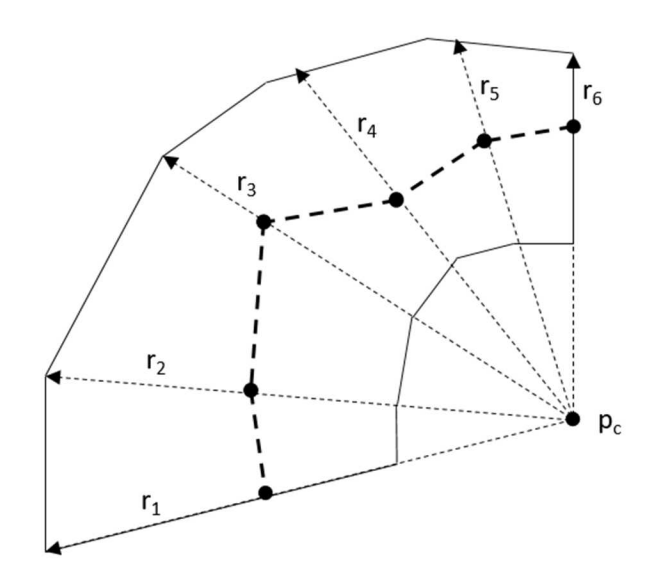


Fig. 1. Parametric definition of material interface geometry.

The derivation of geometric sensitivities will focus on the movement of individual control points and their effect on the local interface. To be more specific, we will examine the area between any two adjacent rays in Figure 1 and how the associated pair of control points affects the local geometry and derived quantities. To that end we arbitrarily choose to focus on the region between r₂ and r₃ to illustrate our derivation. That region is depicted in Figure 2, in which we have added more details necessary for our We relabel rays r_2 and r_3 as **b** and **t**, respectively, to emphasize the generality of our analysis. We depict points p_1 through p_{N+1} (in this figure N=4), placed equidistantly along the material interface; our analysis will examine the limit as N increases. At times we will refer to p₁ and p_N as p_b and p_t. We also depict points p_{l1} through p_{ln} and p_{r1} through p_{m} (with additional "b" and "t" labels) along the left and right region boundaries; their locations are defined by rays emanating from the central point and passing through the points on the interface. A subtle observation to note is that as p_b and p_t move along their rays due to changing geometries, the points in between will follow a path that differs from the rays we depict, which is a consequence of the requirement that they be equidistant along the interface; this will affect our analysis. We must emphasize that these additional points only appear in our analysis for the sake of defining subregions and do not define or constrain the geometry beyond what was depicted in Figure 1. A subregion like that depicted in Figure 2 may be thought of as a "building block" or "unit cell" for the design of the shield; increasing the number (while decreasing the size) of these subregions through the addition of more control points may improve the quality of the design.

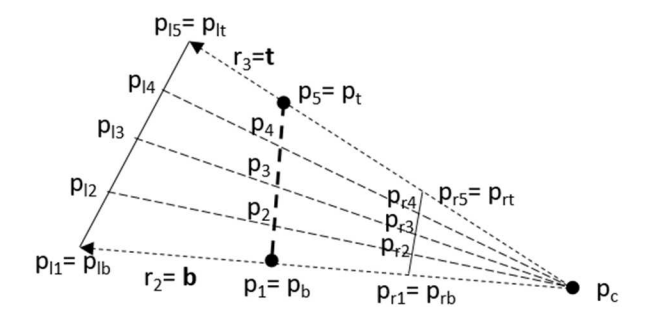


Fig. 2. Depiction of analysis points in region defined by two control points.

To continue our analysis, we will again focus on certain details. We arbitrarily pick the volume bounded by points p_3 and p_4 in Figure 2, which we depict in Figure 3 with some details omitted and others added. Here we show two control volumes to the left and right of the interface which we have defined by adding line segments that are approximately perpendicular to the two rays (the error in the approximation will tend to zero as N increases). The line segments define a new (x', y') coordinate system. Note that these line segments will not in general become colinear with the material boundaries as N increases.

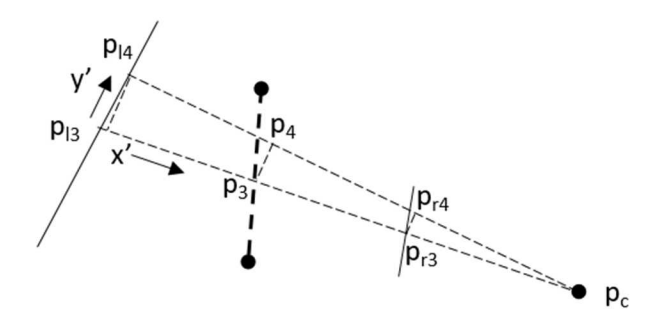


Fig. 3. Definition of differential control volumes.

With the above geometric definitions, we may now proceed with our sensitivity derivations. The requirement that the numbered points on the interface in Figure 2 be equally spaced yields:

$$\vec{p}_n = \vec{p}_b + \frac{n-1}{N} (\vec{p}_t - \vec{p}_b)$$
 (10)

To simplify some aspects of our analysis we define

$$n' = \frac{n-1}{N} \tag{11}$$

n' will vary between 0 and 1. This yields:

$$\vec{p}_n = (1 - n')\vec{p}_b + n'\vec{p}_t \tag{12}$$

We introduce h_b and h_t , the distance of the control points from the central point, with the following definitions:

$$\vec{p}_b = \vec{p}_c + h_b \vec{b} \tag{13a}$$

$$\vec{p}_t = \vec{p}_c + h_t \vec{t} \tag{13b}$$

where we also define \vec{b} and \vec{t} to be unit vectors.

We express the location of each point p_n (as it moves due to control point motion) in terms of the control and central points as well as its unperturbed location:

$$\tilde{x}_{n} = \frac{1}{d} \begin{pmatrix} (x_{b}y_{t} - y_{b}x_{t})(x_{c} - x_{n}) - \\ (x_{b} - x_{t})(x_{c}y_{n} - y_{c}x_{n}) \end{pmatrix}$$
(14a)
$$\tilde{y}_{n} = \frac{1}{d} \begin{pmatrix} (x_{b}y_{t} - y_{b}x_{t})(y_{c} - y_{n}) - \\ (y_{b} - y_{t})(x_{c}y_{n} - y_{c}x_{n}) \end{pmatrix}$$
(14b)
$$d = (x_{b} - x_{t})(y_{c} - y_{n}) - \\ (y_{b} - y_{t})(x_{c} - x_{n})$$
(14c)

We substitute Eq. (13a) into Eqs. (14) to express \tilde{x}_n and \tilde{y}_n in terms of h_b :

$$\tilde{x}_{n} = \frac{1}{d} \left((x_{c} + h_{b}b_{x})y_{t} - (y_{c} + h_{b}b_{y})x_{t})(x_{c} - x_{n}) - (x_{c} + h_{b}b_{x}) - x_{t})(x_{c}y_{n} - y_{c}x_{n}) \right)$$

$$\tilde{y}_{n} = \frac{1}{d} \left((x_{c} + h_{b}b_{x})y_{t} - (y_{c} + h_{b}b_{y})x_{t})(y_{c} - y_{n}) - (y_{c} + h_{b}b_{y}) - y_{t})(x_{c}y_{n} - y_{c}x_{n}) \right)$$

$$d = ((x_{c} + h_{b}b_{x}) - x_{t})(y_{c} - y_{n}) - ((y_{c} + h_{b}b_{y}) - y_{t})(x_{c} - x_{n})$$

$$(15b)$$

Taking derivatives with respect to h_b yields

$$\frac{\partial \tilde{x}_n}{\partial h_b} = \frac{1}{d} \left[\left(b_x y_t - b_y x_t \right) (x_c - x_n) - b_x (x_c y_n - y_c x_n) \right] - \frac{x_n}{d} \left[b_x (y_c - y_n) - b_y (x_c - x_n) \right]$$
(16a)

$$\frac{\partial \tilde{y}_n}{\partial h_b} = \frac{1}{d} \left[\left(b_x y_t - b_y x_t \right) (y_c - y_n) - b_y (x_c y_n - y_c x_n) \right] - \frac{y_n}{d} \left[b_x (y_c - y_n) - b_y (x_c - x_n) \right]$$
(16b)

We obtain similar expressions for $\frac{\partial \tilde{x}_n}{\partial h_t}$ and $\frac{\partial \tilde{y}_n}{\partial h_t}$. We also will need the directional derivative of each of the points with respect to the (x', y') coordinate system:

$$\nabla_{nc,b}\vec{p}_n = \left[\frac{\partial x_n}{\partial h_b} \frac{\partial y_n}{\partial h_b}\right]^T \cdot \frac{\vec{p}_n - \vec{p}_c}{|\vec{p}_n - \vec{p}_c|}$$
(17)

The volumes of the regions to the left and right of the material interface are given by

$$V_l = \frac{1}{2} |(\vec{p}_t - \vec{p}_{lb}) \times (\vec{p}_{lt} - \vec{p}_b)|$$
 (18a)

$$V_r = \frac{1}{2} |(\vec{p}_{rt} - \vec{p}_b) \times (\vec{p}_t - \vec{p}_{rb})|$$
 (18b)

The derivatives of the volumes with respect to geometry changes are:

$$\frac{\partial V_l}{\partial h_b} = -\frac{\partial V_r}{\partial h_b} = -\frac{1}{2} \left| \vec{b} \times (\vec{p}_t - \vec{p}_b) \right| \quad (19a)$$

$$\frac{\partial V_l}{\partial h_t} = -\frac{\partial V_r}{\partial h_t} = -\frac{1}{2} \left| \vec{t} \times (\vec{p}_t - \vec{p}_b) \right| \quad (19b)$$

$$\frac{\partial V_l}{\partial h_t} = -\frac{\partial V_r}{\partial h_t} = -\frac{1}{2} \left| \vec{t} \times (\vec{p}_t - \vec{p}_b) \right| \quad (19b)$$

With the above expressions we can now address transport sensitivities. We will show here some of our derivation with respect to the collision operator, which is given by

$$C\psi = \sum_{n} [H(x' - x'_{p_{ln}}) - H(x' - x'_{p_{n}})] [H(y' - y'_{p_{n}}) - H(y' - y'_{p_{n}})] \sum_{m} p_{ml} (\sigma_{t,g,m,l} - \sigma_{\delta,gg,m,l}) \psi_{g} + \sum_{n} [H(x' - x'_{p_{n}}) - H(x' - x'_{p_{rn}})] [H(y' - y'_{p_{n}}) - H(y' - y'_{p_{n+1}})] \sum_{m} p_{mr} (\sigma_{t,g,m,r} - \sigma_{\delta,gg,m,r}) \psi_{g}$$

$$(20)$$

The derivative of the collision operator with respect to the location of the bottom control point is given by:

$$\frac{\partial \mathcal{C}}{\partial h_{b}} = \sum_{n} \delta(x' - x'_{p_{n}}) \nabla_{nc,b} \vec{p}_{n} \left[H \left(y' - y'_{p_{n}} \right) - H \left(y' - y'_{p_{n+1}} \right) \right] \sum_{m} p_{ml} \left(\sigma_{t,g,m,l} - \sigma_{\delta,gg,m,l} \right) \\
- \sum_{n} \delta(x' - x'_{p_{n}}) \nabla_{nc,b} \vec{p}_{n} \left[H \left(y' - y'_{p_{n}} \right) - H \left(y' - y'_{p_{n+1}} \right) \right] \sum_{m} p_{mr} \left(\sigma_{t,g,m,r} - \sigma_{\delta,gg,m,r} \right) \tag{21}$$

With the above we may derive the contribution of the collision term to the transport response sensitivity:

$$\begin{split} \frac{\partial R}{\partial h_b} &= -\langle \psi_g^{\dagger}, \left(\frac{\partial C}{\partial h_b}\right) \psi_{g'} \rangle \\ &= -\int_{V} dV \sum_{g} \int_{4\pi} d\Omega \, \psi_g^{\dagger}(r, \Omega) \sum_{n} \delta(x') \\ &- x'_{p_n} \nabla_{nc,b} \vec{p}_n \left[H\left(y' - y'_{p_n}\right) - H\left(y' - y'_{p_{n+1}}\right) \right] \sum_{m} p_{ml} \left(\sigma_{t,g,m,l}\right) \\ &- \sigma_{\delta,gg,m,l} \psi_g(r, \Omega) \\ &+ \int_{V} dV \sum_{g} \int_{4\pi} d\Omega \, \psi_g^{\dagger}(r, \Omega) \sum_{n} \delta(x') \\ &- x'_{p_n} \nabla_{nc,b} \vec{p}_n \left[H\left(y' - y'_{p_n}\right) - H\left(y' - y'_{p_{n+1}}\right) \right] \sum_{m} p_{mr} \left(\sigma_{t,g,m,r}\right) \\ &- H\left(y' - y'_{p_{n+1}}\right) \psi_g(r, \Omega) \end{split}$$

Taking the limit as $N \to \infty$ yields the collision contribution to the transport sensitivity with respect to movement of one of the control points for one subregion:

$$\lim_{N\to\infty} \frac{\partial R}{\partial h_b} = -\sum_{g} \sum_{m} p_{ml} (\sigma_{t,g,m,l} - \sigma_{\delta,gg,m,l}) \int_{4\pi} d\Omega \int_{\partial D_l} ds \vec{\iota}' \cdot \vec{n} \nabla_{nc,b} \vec{p}_n \psi_g^{\dagger}(s,\Omega) \psi_g(s,\Omega)$$

$$+ \sum_{g} \sum_{m} p_{mr} (\sigma_{t,g,m,r} - \sigma_{\delta,gg,m,r}) \int_{4\pi} d\Omega \int_{\partial D_r} ds \vec{\iota}' \cdot \vec{n} \nabla_{nc,b} \vec{p}_n \psi_g^{\dagger}(s,\Omega) \psi_g(s,\Omega)$$

$$\cdot \vec{n} \nabla_{nc,b} \vec{p}_n \psi_g^{\dagger}(s,\Omega) \psi_g(s,\Omega)$$

$$(23)$$

Analogous expressions are obtained for the scattering and response operators. Their sum yields the overall transport sensitivity of the desired response to movement of one of the control points on the interface between two constant-density material regions.

We note that the term $\vec{\iota}' \cdot \vec{n} \nabla_{nc,b} \vec{p}_n$ in Eq. (23) appears to be the surface transformation function described in Ref. 11, which defines the magnitude of the perturbation of a given point on a surface in the direction of the surface normal. Our function consists of two components. The term $\nabla_{nc,b}\vec{p}_n$ is related to the distance that a surface point is from the relevant control point and varies from zero to one. The term $\vec{\iota}' \cdot \vec{n}$ accounts for the fact that in our analysis the surface points do not move along the surface normal.

III. RESULTS

In our previous work we implemented transport sensitivities in postprocessing tools for the SCEPTRE deterministic radiation transport code, which includes adjoint capabilities. These sensitivities were incorporated into an analysis process that includes Dakota optimization algorithms; we used the NPSOL solver. In the present work we have incorporated our new geometric sensitivities into that workflow. The use of complicated two-dimensional geometries requires generation of finite element meshes, which we handle with the Cubit mesh generator 14 to obtain meshes with triangular elements.

As an example of our design optimization tools we examine the problem that is depicted in Figure 4. Sensitive components to be protected are within a 10" x 10" box. Two of the sides of the box consist of 50 mils of aluminum. On one side we provide 2" of aluminum, meant to represent the presence of a larger structure such as a satellite body. On the final side we provide ½" of aluminum, meant to represent other equipment or electronics boxes. asymmetry is intended to illustrate how the design tool adjusts to the environment. We choose to examine the proton environment for a circular orbit at 2000 km altitude as defined by the AP8 model in Spenvis, 15 which is stressing enough to clearly show the behavior of our algorithm. This environment is isotropically incident on all sides of the problem. For our current purposes we neglect the electron environment, both because the proton environment dominates the response and because we use a simple model for proton physics that allows for faster runtimes.

Inside the box are four silicon components near the corners and one component (or component region) in the center. For all the components we perform forward and adjoint runs with void in those regions to avoid selfshielding effects, with later postprocessing determining the response of each silicon component from the unperturbed radiation field. On the inside surface of the box is one shielding region, and surrounding the central component is a second shielding region. The intention is to provide a greater level of shielding to the central component(s), perhaps due to a higher sensitivity to radiation. Each shielding region is defined by eight points, which are free to move along the arrows to make that portion of the shield thinner or thicker, thus yielding two 8-sided polygons whose shapes we need to determine. (The mesh resolution will in general be finer than this parametrization, but the shield surfaces will still be defined by eight line segments.) The choice of only sixteen total control points is arbitrary; adding more may improve the design but does nothing to improve the accuracy of the sensitivity calculations. We impose constraints on the points so that the shields do not overlap the structure, components, or each other. For these studies the shields consist of polyethylene at nominal (constant) density.

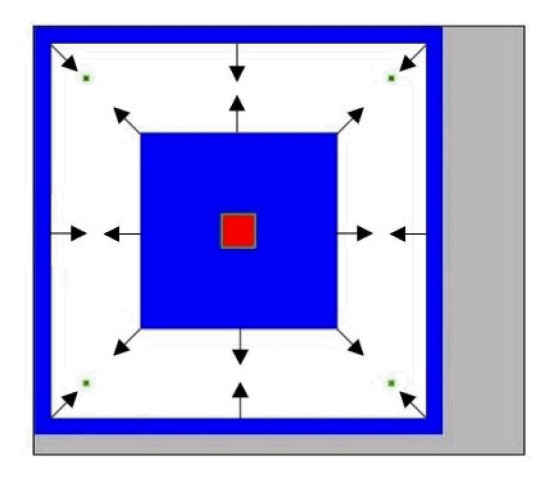


Fig. 4. Initial geometry for design optimizations.

For our initial design study, we impose the requirements that the components in the corners are limited to 100 krad annual dose and the central region is limited to 40 krad. Our objective is to minimize the shielding mass. Since this problem consists of five responses and sixteen design parameters we will need to evaluate 80 sensitivities at each design point. Starting with the initial design in Figure 4, our optimizer produces the sequence of designs depicted in Figure 5 as it searches for a mass-optimal solution that satisfies the dose and geometric constraints.

We also report our adjoint-based sensitivities and finite-difference-based sensitivities for the dose to the center component (for relative step sizes of 0.1, 0.01, and 0.001) in Table I as evaluated for the final design in Figure 5d. In the table the points are labeled according to the associated ray (numbered counter-clockwise starting in the lower-left corner of Figure 4) and the shield (p1 for the outer shield and p2 for the inner shield).

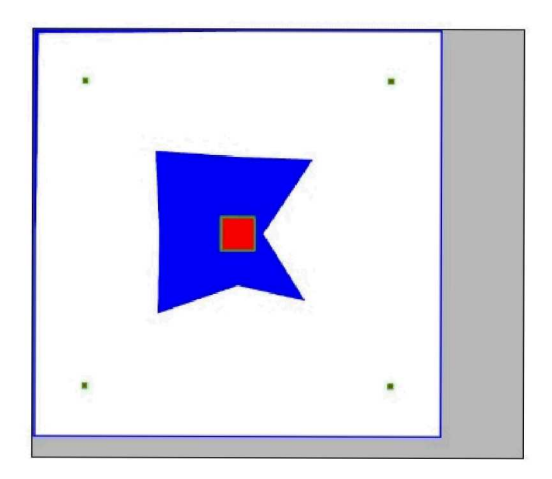


Fig. 5a. Second design iteration, 40 krad limit on central region.

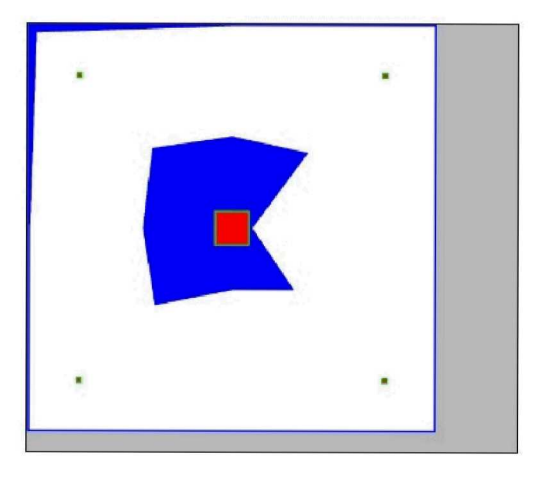


Fig. 5b. Third design iteration, 40 krad limit on central region.

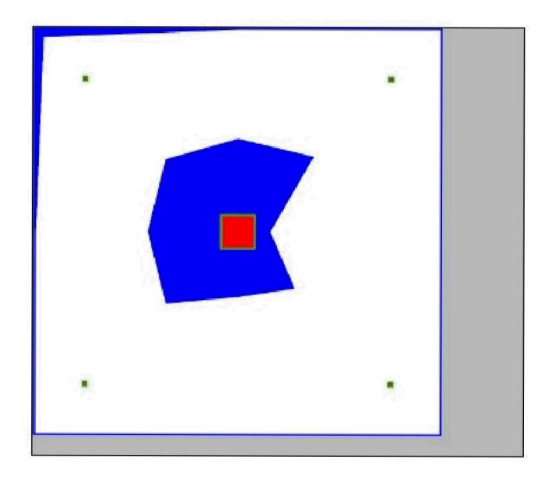


Fig. 5c. Fourth design iteration, 40 krad limit on central region.

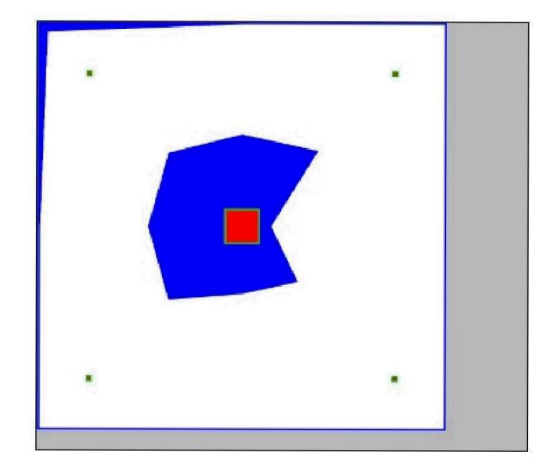


Fig. 5d. Fifth (and final) design iteration, 40 krad limit on central region.

Table I. Adjoint and	finite difference sensitivities	for design of Figure 5d.

Control point	Adjoint sensitivity (krad/cm)	FD sens. (0.1 step size)	Relative difference	FD sens. (0.01 step size)	Relative difference	FD sens. (0.001 step size)	Relative difference
r1::p1	0.5533	0.5104	0.0775	0.5633	-0.0181	0.3578	0.3533
r2::p1	0.6709	0.6333	0.0561	0.6233	0.0710	0.9644	-0.4374
r3::p1	0.3611	0.3379	0.0643	0.3596	0.0041	0.3549	0.0173
r4::p1	0.2758	0.2728	0.0109	0.3034	-0.0999	0.4305	-0.5606
r5::p1	0.4944	0.4457	0.0984	0.4775	0.0341	0.5857	-0.1847
r6::p1	0.8796	0.8216	0.0659	0.8758	0.0043	1.0354	-0.1772
r7::p1	0.6155	0.5749	0.0660	0.6388	-0.0378	0.6259	-0.0169
r8::p1	0.8694	0.8129	0.0650	0.8539	0.0178	0.7315	0.1586
r1::p2	-0.5798	-0.5379	0.0722	-0.5598	0.0344	0.1695	1.2924
r2::p2	-0.6726	-0.6187	0.0801	-0.5973	0.1119	-1.3661	-1.0311
r3::p2	-0.3359	-0.3264	0.0284	-0.3181	0.0530	-0.0995	0.7039
r4::p2	-0.6286	-0.6161	0.0198	-0.4518	0.2813	-1.1644	-0.8524
r5::p2	-0.4543	-0.4336	0.0455	-0.4173	0.0814	0.4040	1.8892
r6::p2	-0.7885	-0.7324	0.0711	-0.7496	0.0494	-0.8296	-0.0521
r7::p2	-0.6869	-0.6385	0.0705	-0.6520	0.0508	-0.3199	0.5343
r8::p2	-0.7572	-0.6895	0.0895	-0.6040	0.2024	-0.3140	0.5854

We make a few observations about the design and design sequence:

- The sequence of designs appears nearly monotonic with respect to the geometry. This will not always be true for the optimizer we use, which may perform design iterations that are intended to guard against settling on a local rather than a global minimum.
- There is a slight amount of shielding in the upper left portion of the outer shield. This is desirable, since the dose to the component in that corner will slightly exceed requirements if only the aluminum were present. Elsewhere that outer shield has the minimum thickness we allowed to ensure valid mesh creation.
- The inner shield is asymmetric in a manner that is physically plausible, with more shielding facing the thinner aluminum structure and the least facing the thickest aluminum structure.
- The "blockiness" of our design is not an approximation to the geometry; it is the optimal geometry for the number of control points and the placement of their associated rays.

• There are some differences between our adjoint-based sensitivities and those obtained by finite difference calculations. We note that we did not use a highly-resolved mesh for these calculations, so there will be numerical errors in both types of sensitivities, in addition to the usual error of finite-difference estimates. With a more highly resolved mesh we would expect improved agreement with smaller step sizes.

In Figures 6 and 7 we depict the final design produced in two other design studies in which the requirement on the central component is 30 krad and 20 krad, respectively. We observe here that more shielding is supplied as the dose requirement is lowered (as expected), and the shields maintain their asymmetry. For the latter study an interesting phenomenon occurs: all but one of the control points of the inner shield are at their maximum extent, forcing additional shielding in the outer layer. This nicely illustrates how the optimizer respects constraints and adjusts accordingly.

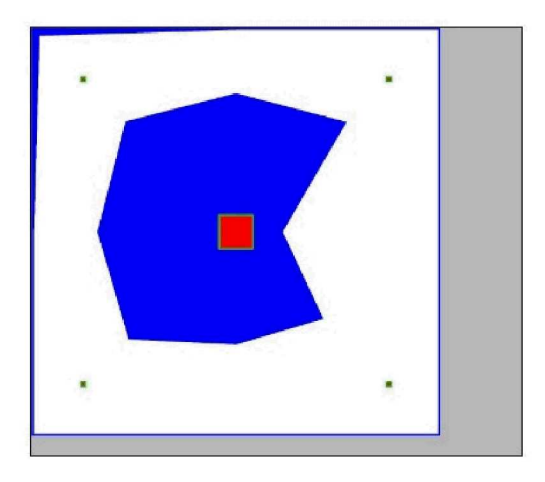


Fig. 6. Final design, 30 krad limit on central region.

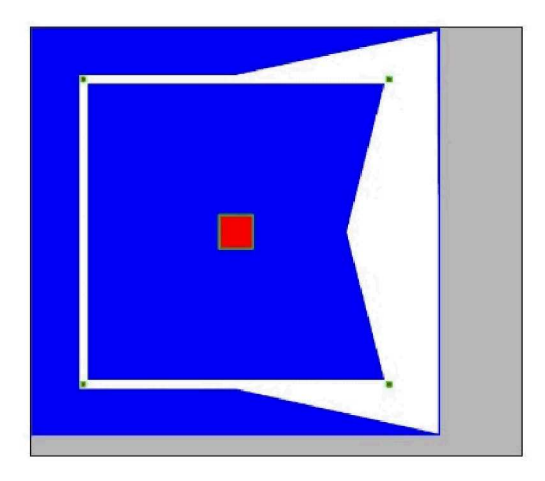


Fig. 7. Final design, 20 krad limit on central region.

IV. CONCLUSIONS

In past work we created a design optimization process for satellite shields in one-dimensional slab geometry that makes use of adjoint-based transport sensitivities. In the present work we have extended that capability to two-dimensional Cartesian geometries. We have derived sensitivities to a general description of geometric changes, incorporated those sensitivities into our design process, and applied the capability to some realistic problems. The design process appears to behave as expected, yielding physically plausible designs that respect dose and geometric constraints.

One strength of our approach is that we can define an arbitrarily complicated geometry (depending on the number of control points we choose) and obtain accurate sensitivity equations for that geometry. The resulting designs will meet the design requirements, although one can potentially improve on them by adding more geometric degrees of freedom. In the results we reported we limited ourselves to sixteen control points, but there is no fundamental reason why we couldn't use more. There will be additional computational costs to determine the sensitivities, but the adjoint formulation allows us to perform just two transport solves per design iteration.

In future work we hope to apply our tools to even more general problems. The problems we examined in this work had proton-only environments; we need to apply our tools to combined proton/electron environments as we have in one-dimensional slab geometries. We reported on design optimization that looked strictly at geometric changes for fixed materials; we need to perform optimization calculations that allow for both geometry and materials changes. Our goal is to create a generally useful design tool that allows analysts to examine a rich design space to help inform engineering decisions for future space missions.

NOMENCLATURE

C =collision operator

 \mathbf{b} = bottom control ray in subregion

 C^{\dagger} = adjoint collision operator

D = spatial domain, discrete angular flux to angular flux moment operator

 $\nabla_{nc,b}\vec{p}_n$ = directional derivative of point p_n

E = particle energy g = energy group index

H = Heaviside function

 h_b = distance along bottom ray to control point

 h_t = distance along top ray to control point

i = region index

L =streaming operator

 L^{\dagger} = adjoint streaming operator

 $\mathcal{L} = Lagrangian$

m = material index

M = angular flux moment to discrete angular flux operator

 Ω = particle direction

p = design parameter

 $p_c = central point$

 $p_b = bottom interface point in subregion$

 $p_n = n$ th interface point in subregion

 $p_{ln} = nth$ left boundary point in subregion

 $p_{\rm rn} = n$ th right boundary point in subregion

 $p_t = top interface point in subregion$

 $p_{m,i}$ = material volume fraction

 ψ = angular flux

 ψ^{\dagger} = adjoint angular flux

q = transport source

 q^{\dagger} = adjoint transport source

r =spatial coordinate

 $r_i = i$ th control ray

 ρ_i = density of region i

R = response to radiation

S = scattering operator

 S^{\dagger} = adjoint scattering operator

 σ_d = dose cross section

 $\sigma_{\delta,g'g,m}$ = group-to group delta scattering cross section

 σ_s = scattering cross section

 σ_t = total cross section

 $\Sigma_{g'g,m}$ = multigroup scattering operator

 $\mathbf{t} = \text{top control ray in subregion}$

 V_i = volume of region i

x' = rotated x-coordinate

 \tilde{x}_n = perturbed x-coordinate of point p_n

y' = rotated y-coordinate

 \tilde{y}_n = perturbed y-coordinate of point p_n

ACKNOWLEDGMENTS

Supported by the Laboratory Directed Research and Development program at Sandia National Laboratories, a multimission laboratory managed and operated by National Technology and Engineering Solutions of Sandia, LLC, a wholly owned subsidiary of Honeywell International, Inc., for the U.S. Department of Energy's National Nuclear Security Administration under contract DE-NA0003525.

REFERENCES

- 1. W.C. FAN, C.R. DRUMM, S.B. ROESKE, and G.J. SCRIVNER, "Shielding Considerations for Satellite Microelectronics," *IEEE Trans. On Nuclear Science*, **43**, *6*, 2790 (1996).
- H. F. STRIPLING, M. ANITESCU, and M. L. ADAMS, "A generalized adjoint framework for sensitivity and global error estimation in time-dependent nuclear reactor simulations," *Annals of Nuclear Energy*, 52, 47 (2013).
- 3. D.E. BRUSS, *Adjoint-Based Uncertainty Quantification for Neutron Transport Calculations*, Ph.D. Dissertation, Texas A&M University (2016).
- 4. JEFFREY A. FAVORITE and KEITH BLEDSOE, "Eigenvalue Sensitivity to System Dimensions," *Annals of Nuclear Energy*, **37**, 522 (2010).
- 5. JEFFREY A. FAVORITE and ESTEBAN GONZALEZ, "Revisiting Boundary Perturbation Theory for Inhomogeneous Transport Problems," *Nuclear Science and Engineering*, **185**, 445 (2017).
- JEFFREY A. FAVORITE, "Nonspherical Perturbations of Spherical Geometries in Transport

- Theory," Nuclear Science and Engineering, 175, 44 (2013).
- 7. JEFFREY A. FAVORITE, "Spherical Shields Perturbed to Ellipsoids in Transport Theory," *Annals of Nuclear Energy*, **65**, 376 (2014).
- 8. KEITH C. BLEDSOE, JEFFREY A. FAVORITE and TUNC ALDEMIR, "Using the Levenberg-Marquardt Method for Solutions of Inverse Transport Problems in One- and Two-Dimensional Geometries," *Nuclear Technology*, **176**, 106 (2011).
- KEITH C. BLEDSOE, MATTHEW A. JESSEE, and JEFFREY A. FAVORITE, "Application of Generalized Linear Least-Squares for Uncertainty Quantification in Inverse Transport Problems," Transactions of the American Nuclear Society, 108, 445 (2013).
- 10. SHAWN D. PAUTZ, BRIAN C. FRANKE, BRIAN M. ADAMS, LAURA P. SWILER and ETHAN L. BLANSETT, "Adjoint-Based Sensitivities for Optimization of Satellite Electron/Proton Shields," Proc. International Conference on Mathematics & Computational Methods Applied to Nuclear Science & Engineering, Jeju, Korea, April 16-20, 2017, American Nuclear Society (2017) (USB).
- 11. F. RAHNEMA, "On the Internal Interface Perturbation," *Annals of Nuclear Energy*, **23**, 1401 (1996).
- S. PAUTZ, B. BOHNHOFF, C. DRUMM and W. FAN, "Parallel Discrete Ordinates Methods in the SCEPTRE Project," Proc. Int. Conf. on Mathematics, Computational Methods and Reactor Physics, Saratoga Springs, NY, May 3-7, 2009, CD-ROM, American Nuclear Society (2009).
- 13. B.M. ADAMS, W.J. BOHNHOFF, K.R. DALBEY, J.P. EDDY, M.S. EBEIDA, M.S. ELDRED, P.D. HOUGH, K.T. HU, J.D. JAKEMAN, K.A. MAUPIN, J.A. MONSCHKE, E.M. RIDGWAY, A. RUSHDI, L.P. SWILER, J.A. STEPHENS, D.M. VIGIL, and T.M. WILDEY, "Dakota A Multilevel Parallel Object-Oriented Framework for Design Optimization, Parameter Estimation, Uncertainty Quantification and Sensitivity Analysis: Version 6.4 User's Manual," SAND2014-4633, Sandia National Laboratories (2016).
- 14. T. BLACKER, S.J. OWEN, M.L. STATEN, R.W. QUADROS, B. HANKS, B. CLARK, T. HENSLEY, R.J. MEYERS, C. ERNST, K. MERKLEY, R. MORRIS, C. MCBRIDE, C. STIMPSON, M. PLOOSTER, and S SHOWMAN, "CUBIT Geometry and Mesh Generation Toolkit 15.3 User Documentation," SAND2017-6895 W, Sandia National Laboratories (2017).

15. "Space Environment Information System (SPENVIS)", http://www.spenvis.oma.be/spenvis, European Space Agency (2016).